

DENSE CO IN MRK 71-A: SUPERWIND SUPPRESSED IN A YOUNG SUPER STAR CLUSTER

M. S. OEY,<sup>1</sup> C. N. HERRERA,<sup>2</sup> SERGIY SILICH,<sup>3</sup> MEGAN REITER,<sup>1</sup> BETHAN L. JAMES,<sup>4</sup> A. E. JASKOT,<sup>5,\*</sup> AND  
GENOVEVA MICHEVA<sup>1</sup>

<sup>1</sup>*Department of Astronomy  
University of Michigan  
1085 South University Ave.*

*Ann Arbor, MI 48109-1107, USA*

<sup>2</sup>*Institut de Radioastronomie Millimétrique  
300 Rue de la Piscine*

*Domaine Universitaire*

*38406, Saint-Martin-d'Hères, France*

<sup>3</sup>*Instituto Nacional de Astrofísica, Óptica y Electrónica  
AP 51*

*72000 Puebla, Mexico*

<sup>4</sup>*Space Telescope Science Institute  
3700 San Martin Drive*

*Baltimore, MD 21218, USA*

<sup>5</sup>*Department of Astronomy  
University of Massachusetts*

*Amherst, MA 01003, USA*

(Received 2017 September 12; Accepted 2017 October 8)

ABSTRACT

We report the detection of CO( $J = 2 - 1$ ) coincident with the super star cluster (SSC) Mrk 71-A in the nearby Green Pea analog galaxy, NGC 2366. Our NOEMA observations reveal a compact,  $\sim 7$  pc, molecular cloud whose mass ( $10^5 M_{\odot}$ ) is similar to that of the SSC, consistent with a high star-formation efficiency, on the order of 0.5. There are two, spatially distinct components separated by  $11 \text{ km s}^{-1}$ . If expanding, these could be due to momentum-driven, stellar wind feedback. Alternatively, we may be seeing the remnant infalling, colliding clouds responsible for triggering the SSC formation. The kinematics are also consistent with a virialized system. These extreme, high-density, star-forming conditions inhibit energy-driven feedback; the co-spatial existence of a massive, molecular cloud with the SSC supports this scenario, and we quantitatively confirm that any wind-driven feedback in Mrk 71-A is momentum-driven, rather than energy-driven. Since Mrk 71-A is a candidate Lyman continuum emitter, this implies that energy-driven superwinds may not be a necessary condition for the escape of ionizing radiation. In addition, the detection of the nebular continuum emission yields an accurate astrometric position for the Mrk 71-A. We also detect four other massive, molecular clouds in this giant star-forming complex.

*Keywords:* stars: formation — stars: massive — ISM: bubbles — ISM: molecules — galaxies: starburst  
— galaxies: star clusters: general

Corresponding author: M. S. Oey  
[msoey@umich.edu](mailto:msoey@umich.edu)

\* Hubble Fellow

## 1. INTRODUCTION

How and when do newborn super star clusters (SSCs), like the progenitors of globular clusters, emerge from dense gas and clear their surroundings? The classical model for starburst mechanical feedback holds that stellar winds and supernovae inside SSCs collide and merge to form strong superwinds (Chevalier & Clegg 1985). This hot ( $\gtrsim 10^7$  K), shock-heated gas carries off most of the newly synthesized heavy elements produced by the massive stars and their supernovae. In dwarf galaxies, these metals could be ejected into the intergalactic medium, retarding chemical evolution of the host galaxy. However, more recent developments in our understanding of both massive star feedback and chemical abundance patterns suggest that this picture is more complex. Theoretical work suggests that catastrophic cooling and large ambient gas pressure may inhibit the development of superwinds and wind-driven superbubbles (Silich et al. 2007; Silich & Tenorio-Tagle 2017), and radiation feedback is suggested to be important in the youngest and densest clusters (e.g., Freyer et al. 2003; Krumholz & Matzner 2009). On the observational side, multiple stellar populations with differing abundances are now ubiquitous in individual globular clusters (e.g., Gratton et al. 2012), suggesting that star formation may have recurred in these objects. So then what factors dominate the interaction between a brand-new SSC and its gaseous environment? Observations of newly born SSCs that are still clearing their gas are vital to revealing these processes. Here, we present remarkable CO observations revealing that a young,  $10^5 M_{\odot}$  SSC, Mrk 71-A, located in a relatively clear environment, nevertheless coexists with an extremely compact, molecular cloud of comparable mass.

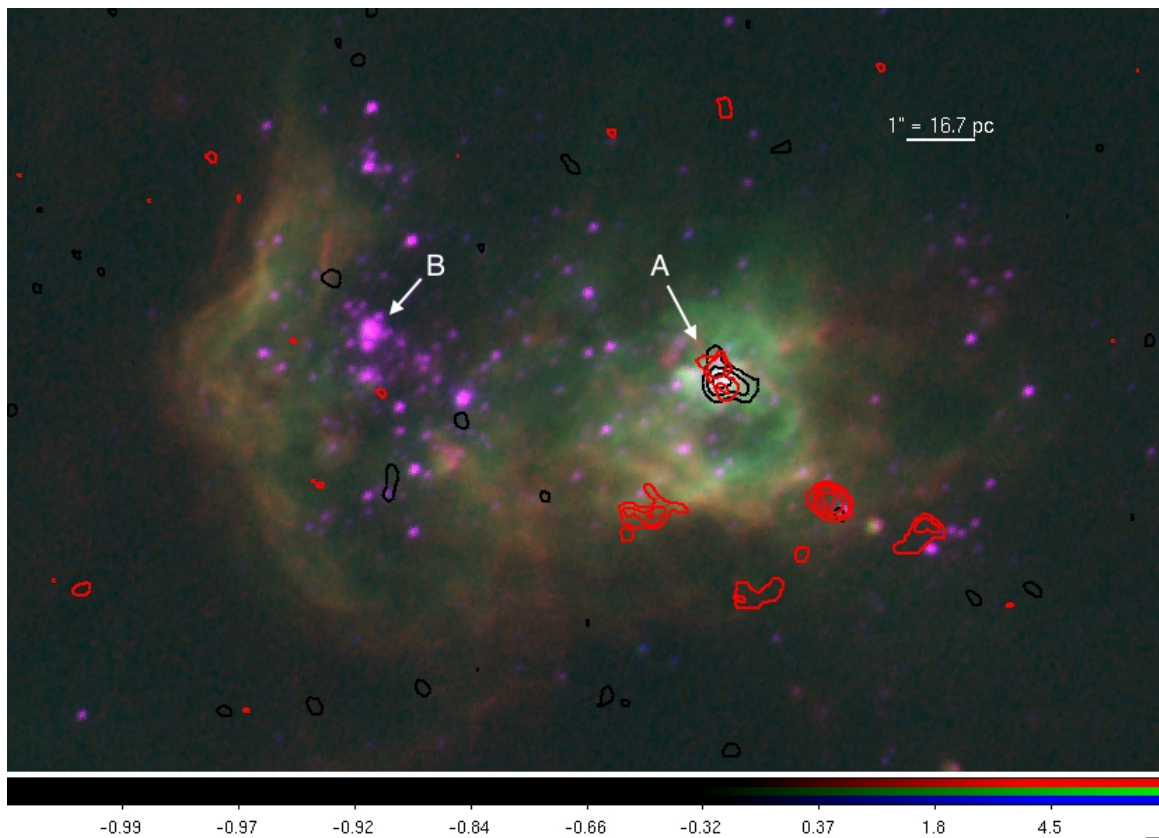


**Figure 1.** Composite image of Mrk 71 using *HST*/WFC3 data from James et al. (2016). Red, green, blue correspond to [O II]  $\lambda 3727$  (F373N), [O III]  $\lambda 5007$  (F502N), and blue continuum (F438W), respectively. Red contours show line emission of CO(2–1) detected with NOEMA, integrated over  $62 - 90.6 \text{ km s}^{-1}$ , selecting pixels with emission  $> 2\sigma$ . Contour levels are 0.03, 0.06, 0.09, 0.12, and 0.15 Jy/beam km/s. Black contours show the corresponding continuum emission integrated over 3.6 GHz, excluding 10 MHz of line emission, with contour levels at  $2, 3, \text{ and } 4 \times 10^{-4}$  Jy/beam. North is up, east to the left.

Mrk 71 is a well-studied starburst complex in the nearby barred Im galaxy, NGC 2366, at a distance of 3.4 Mpc (Tolstoy et al. 1995). It hosts two SSCs, Mrk 71-A and B (Figure 1). Mrk 71-B is an exposed cluster with mass  $1.5 \times 10^4 M_{\odot}$  (Micheva et al. 2017) and age of 3 – 5 Myr constrained by the presence of classical WR stars (Drissen

et al. 2000). Mrk 71-A, however, strongly dominates the complex, producing about ten times more ionizing photons, implying an SSC stellar mass of  $M_* = 1.4 \times 10^5 M_\odot$  (Micheva et al. 2017; Drissen et al. 2000). To date, Mrk 71-A has only been detected as a compact, extreme excitation H II region. No stellar features are spectroscopically detected, but strong nebular continuum is observed, including inverse Balmer and Paschen jumps (e.g., González-Delgado et al. 1994; Guseva et al. 2006). It is marginally spatially resolved with the *Hubble Space Telescope* (HST), implying a radius of  $\lesssim 1$  pc. Thus Mrk 71-A has an extremely high nebular surface brightness and is remarkably similar to a massive, ultracompact H II region (Drissen et al. 2000), but hosting a  $10^5 M_\odot$  newly-formed, embedded cluster.

The Mrk 71/NGC 2366 system is especially interesting owing to its status as a local analog to extreme “Green Pea” galaxies. These are objects at  $z \sim 0.2$  (Cardamone et al. 2009) that represent a compelling class of local, candidate Lyman continuum-emitting galaxies. They are low-mass, compact starbursts characterized by high ratios of  $[\text{O III}]\lambda 5007/[\text{O II}]\lambda 3727 \gtrsim 5$  and  $\text{H}\beta$  equivalent widths  $> 100 \text{ \AA}$ , and they are in many ways good analogs of high-redshift starbursts. We showed that among these objects, those with the most extreme ionization parameters are strong candidate Lyman continuum emitters (LCEs; Jaskot & Oey 2013). Our prediction was dramatically confirmed when Izotov et al. (2016a, b) detected Lyman continuum emission from all five of their targeted Green Peas, thereby instantly doubling the number of confirmed local LCEs. The properties of Mrk 71 are quantitatively consistent with those of Green Peas and, like those objects, Mrk 71 shows a variety of features that are consistent with optically thin Lyman continuum (Micheva et al. 2017). Thus, Mrk 71/NGC 2366 may also offer a unique opportunity to study what properties facilitate the escape of ionizing radiation.

## 2. CO OBSERVATIONS

We obtained observations of Mrk 71 on 2016 December 14 and 15, with the Northern Extended Millimeter Array (NOEMA) at Plateau de Bure, in the CO ( $J = 2 - 1$ ) line at 230.538 GHz, with a local standard of rest velocity of  $90 \text{ km s}^{-1}$ . The observations were carried out with 8 antennae in Configuration A, with baselines between 45 m and 760 m. We used the Widex correlator, with total bandwidth of 3.6 GHz and native spectral resolution  $1.95 \text{ MHz}$  ( $2.6 \text{ km s}^{-1}$ ). The quasars 0716+714 and 0836+710 were observed as phase and amplitude calibrators, 3C 84 as band-pass calibrator, and the stars MWC 349 and LkHA 101 (1.91 Jy and 0.56 Jy at 230.5 GHz) as absolute flux calibrators. System temperatures were between 90 and 240 K, and the precipitable water vapor  $\sim 2\text{--}3$  mm. Data reduction, calibration and imaging were performed with CLIC and MAPPING software of GILDAS<sup>1</sup>, using standard procedures. Images were reconstructed using natural weighting, resulting in a synthesized beam of  $0''.48 \times 0''.35$  (PA=55.8°) and rms noise in the CO map of  $2.2 \text{ mJy beam}^{-1}$  in a  $2.6 \text{ km s}^{-1}$  channel. The continuum map has rms noise of  $75 \mu\text{Jy beam}^{-1}$ .

The  $22''$  field of view encompasses the entire Mrk 71 complex. Figure 1 shows a 3-color image using HST/WFC3 data in  $[\text{O II}]\lambda 3727$  (F373N),  $[\text{O III}]\lambda 5007$  (F502N), and blue continuum (F438W) superposed with red contours showing the continuum emission at 231 GHz within a bandwidth of 3.6 GHz, and black contours showing line emission of CO(2–1). Five sources are detected, one of which we determine coincides with Mrk 71-A, as follows. The HST absolute astrometry has uncertainty of  $\sim 1''$ , while the NOEMA astrometry is good to  $0.05''$ . However, since Mrk 71-A is a strong nebular continuum source, our detected mm source must correspond to this target. Flux densities for Mrk 71-A from the VLA reported at 3.6, 6, and 20 cm by Chomiuk & Wilcots (2009) with angular resolution of  $3.7''$  yield a spectral index of  $-0.13$ , indicating a thermal H II region continuum. Our NOEMA continuum observation of  $0.71 \text{ mJy}$  is less than the predicted value of  $3.35 \text{ mJy}$  extrapolated from the VLA data. However, we only detect the high surface-brightness core of Mrk 71-A in the NOEMA continuum (Figure 1). Since the VLA beam diameter is about  $10\times$  larger than for our observations, the extended nebular emission dominates the flux in the large aperture. The non-detection of any other NOEMA continuum source within the VLA beam and the agreement of the flux densities with a thermal power-law index therefore indicate that the observed emission must be due to the same source, Mrk 71-A. In Figure 1, we have therefore aligned the data so that the mm continuum peak necessarily coincides with the optical H II region centroid. The position for Mrk 71-A is thus:  $07^h 28^m 42^s.716$ ,  $+69^\circ 11' 22''.07$  (J2000) with uncertainty of  $0.05''$ .

Figure 1 shows a detection of CO(2–1) coincident with the thermal continuum source. The first two lines of Table 1 show the source parameters based on calculating the flux above  $2\sigma$  and  $3\sigma$ . Mrk 71 has  $12 + \log(\text{O}/\text{H}) = 7.89$  (Izotov et al. 1997). For this low, SMC-like value, the transition ratio  $R_{\text{CO}} \equiv \text{CO}(2-1)/\text{CO}(1-0)$  is  $\gtrsim 1$ , observed in SMC H II regions (Rubio et al. 1993), and similar ratios are seen in 30 Doradus ( $R_{\text{CO}} = 0.95 \pm 0.06$ ; Sorai et al. 2001). Thus,

<sup>1</sup> <http://www.iram.fr/IRAMFR/GILDAS/>

**Table 1.** CO(2–1) Observations of Mrk 71

Cloud <sup>a</sup>	Size pc	$v_{\text{LSR}}$ [km/s]	$\Delta v$ <sup>b</sup> [km/s]	Peak [mJy]	Flux [mJy km/s]	$I_{\text{CO}}$ [K km/s]	Flux mass <sup>c</sup> [ $10^4 M_{\odot}$ ]	Virial mass <sup>d</sup> [ $10^4 M_{\odot}$ ]
1	9.0	77.7±0.7	15.9±1.7	10.7 ±1.0	181±25	13±2	14±2	22±5
1 (>3 $\sigma$ )	5.5	78.1±0.7	16.1±1.7	7.7±0.7	131±18	15±2	10±1	14±3
1-blue	10.7	73.6±0.7	6.3±1.5	12.0±2.0	80±24	5.9±1.7	6.2±1.8	4.0±2.0
1-red	5.4	82.6±1.2	9.0±2.8	9.3±1.4	89±31	6.6±2.3	6.9±2.4	4.2±2.6
2	8.5	78.7±0.8	15.3±2.0	13.1±1.4	213±36	12±2	16±3	19±5
3	9.7	75.0±0.4	8.4±1.0	20.1±2.0	180±28	14±3	14±2	5.7±1.3
4	8.9	79.1±0.4	7.6±1.0	17.0±2.0	137±25	9±2	11±2	4.6±1.3
5	8.6	73.5±0.4	6.1±0.9	15.6±1.9	101±19	7±3	7.8±1.5	3.0±0.9

<sup>a</sup>Values measured from pixels with fluxes  $> 2\sigma$ , unless otherwise specified. “Blue” and “red” denote the components of Cloud 1.

<sup>b</sup>FWHM of CO line.

<sup>c</sup>Mass based on CO intensity estimated using  $X_{\text{CO}} = 50 \times 10^{20} \text{cm}^{-2} (\text{K km/s})^{-1}$ . The errors shown correspond to measurement uncertainty only, while  $X_{\text{CO}}$  is uncertain to a factor of a few.

<sup>d</sup>Virial mass calculated as  $190 r(\text{pc}) \times [\Delta v(\text{km/s})]^2$  (MacLaren et al. 1988), where the cloud radius  $r$  is half the value in Column 2. Errors shown are estimated only from the error in the fit of  $\Delta v$ .

we take  $R_{\text{CO}} = 1$ . The CO-to-H<sub>2</sub> conversion factor from CO(1–0),  $X_{\text{CO}}$ , is quite uncertain at this low metallicity; based on studies of other blue compact dwarfs (Amorín et al. 2016; Bolatto et al. 2013; Leroy et al. 2011), we adopt  $X_{\text{CO}} = 50 \times 10^{20} \text{cm}^{-2}/(\text{K km s}^{-1})$ , yielding a total molecular gas mass of  $M_g = 1 \times 10^5 M_{\odot}$ . This cloud mass is similar to our estimated mass of  $M_{\star} = 1.3 \times 10^5 M_{\odot}$  for the enshrouded SSC, based on the H $\alpha$  luminosity (Micheva et al. 2017). Taken together, the masses agree well with the virial mass (Table 1).

However, we caution that  $X_{\text{CO}}$  is uncertain to a factor of a few. If the system is not virial, the cloud mass may be a substantial upper limit. On the other hand, the Mrk 71-A system strongly resembles the molecular cloud NGC 5253-D1, which is associated with a radio supernova and SSC (Turner et al. 2015, 2017). Turner et al. (2017) suggest that the SSC may be overluminous for its mass; this may also apply to Mrk 71-A, where we indeed suggested possible evidence for very massive stars (VMS) of  $> 100 M_{\odot}$  (Micheva et al. 2017). If these dominate the SSC luminosity, then its stellar mass would be overestimated. In any case, the relative masses of the cloud and SSC are consistent with an extremely high star-formation efficiency (SFE), on the order of 0.5. This is again similar to NGC 5253-D1 (Turner et al. 2015) and SGMC 4/5-B1 in the Antennae (Herrera & Boulanger 2017).

We detect four other sources at  $> 2\sigma$ . All are in the region south of Knot A, within 50 pc of the SSC (Figures 1, 2), with no continuum detections. These are all molecular clouds similar in mass to Knot A, with parameters given in Table 1. Source 2 has a large line width, similar to Source 1 (Figure 2). Source 3 has the highest peak intensity, but shows no evidence of star formation.

### 3. FEEDBACK IN MRK 71-A

Young SSCs are thought to clear their environment through massive star feedback, but the details of how and when this takes place are poorly understood. Alternatively, extremely high SFE may itself account for some gas clearing (Kruijssen 2012). Typically, feedback is characterized by a model in which the mechanical energy of stellar winds and supernova ejecta is thermalized, leading to a high central overpressure. The hot, shocked gas flows away from the cluster as a superwind, colliding with the ambient ISM and forming a bubble that grows in an energy-conserving mode (Weaver et al. 1977; Mac Low & McCray 1988). Through photoionization and radiation pressure, Lyman continuum (LyC) photons from the hot, massive stars also generate feedback effects that can be of comparable magnitude to mechanical feedback, especially for the youngest and most compact SSCs (e.g., Freyer et al. 2003; Krumholz & Matzner 2009;

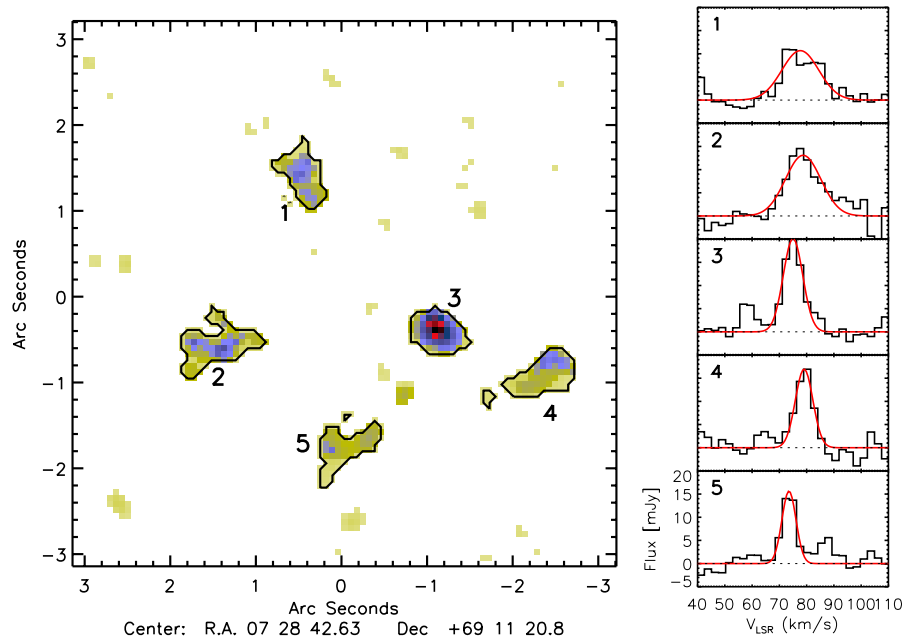


**Figure 2.** Intensity map and CO(2–1) line profiles for all newly detected CO clouds shown in Figure 1. Source 1 is Mrk 71-A.

Dale 2015, but see Silich & Tenorio-Tagle 2013; Martínez-González et al. 2014). It is essential to understand how these processes interact to determine the duration of the clearing process, and how the gas properties and conditions evolve. Mrk 71-A offers a unique opportunity to test feedback theories. Its mass, compactness, and extreme youth place it in the critical regime where the dominant processes are unclear, and its proximity, with an unobscured line of sight, allows high quality estimates of the physical parameters for quantitative modeling.

The observed CO(2–1) emission line is double-peaked, with a velocity separation of  $11.1 \text{ km s}^{-1}$  (Figure 3a). Figure 3b shows the spatial distribution of the two components, showing that they are not fully coincident. At face value, the peaks are offset from the continuum peak by about 1.7 pc ( $0.10''$ ) and 6.0 pc ( $0.36''$ ) in projection, for the blue and red components, respectively (Figure 3b), although the beam size should be noted. These may be separate, distinct clouds, with 7 pc ( $0.42''$ ) separation, in projection. Both components appear to be extended, although the red component is marginally resolved at the  $3\sigma$  level. The blue component is resolved, and encompasses the continuum peak in projection, allowing for the possibility that much molecular gas is cospatial with the SSC stars. The kinematics, line fluxes, and implied molecular masses of the two components are given in Table 1, based on gaussian fitting of the spectral lines.

To explain the presence of  $10^5 M_{\odot}$  of molecular gas at such close quarters to the young SSC, a first impression is that the gas could simply be the cluster’s natal material that is still in the process of being destroyed through conventional mechanical and radiation feedback. However, in high-density star-forming conditions, these feedback processes are counteracted by radiative cooling and larger intra-cloud gas pressure. Our new observations support this dynamic, also seen in M82-A1 (Smith et al. 2006).

If the two CO components represent an outflow, they could correspond to mechanical feedback with an expansion radius and velocity of  $R \sim 3.5 \text{ pc}$  and  $v \sim 5 \text{ km s}^{-1}$ , respectively. If the observed molecular gas corresponds to material swept up within a 3.5-pc radius, the total molecular mass of  $M_g \sim 10^5 M_{\odot}$  corresponds to an original uniform density of  $n_0 \sim 2 \times 10^4 \text{ cm}^{-3}$ , a reasonable average value for the dense core of a massive, giant molecular cloud. At these high densities, cooling dictates that either the wind cannot form (Silich & Tenorio-Tagle 2017), or the system transitions rapidly from the energy-dominated to momentum-dominated regime (e.g., Mac Low & McCray 1988). The age,  $t_6$  (Myr), of a momentum-driven shell can be estimated as  $0.5R/v = 0.3 \text{ Myr}$ . The growth of the shell radius  $R$  is given

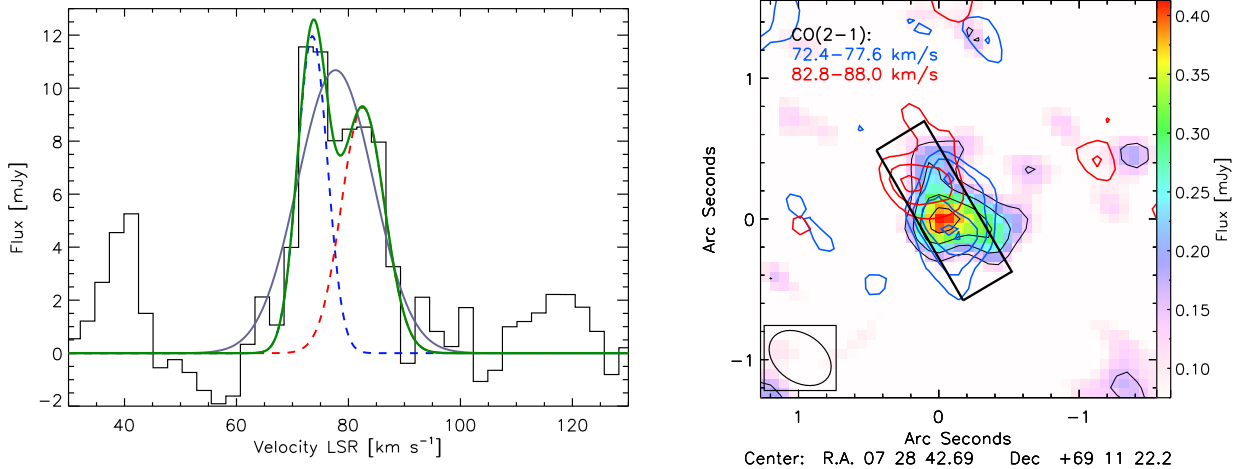


**Figure 3.** Panel *a* (left) shows the CO(2–1) line profile for Mrk 71-A, extracted from an area of  $0''.68$  size, defined as the emission  $> 2\sigma$  in the map integrated over  $72 - 88 \text{ km s}^{-1}$ . The two fitted gaussian components are shown with dashed blue and red lines, and the single fitted gaussian with the solid green line. Panel *b* (right) shows the spatial distribution of the two components in blue and red contours, corresponding to the respective kinematic components in the left panel. The continuum flux is indicated by the color scale bar. The contours for the continuum correspond to  $2, 3, 4,$  and  $5\sigma$  with rms  $0.075 \text{ mJy/beam}$ . The contours for the blue and red components are integrated over  $72.4 - 77.6 \text{ km s}^{-1}$  and  $82.8 - 88.0 \text{ km s}^{-1}$ , respectively, both showing contours starting at  $2\sigma$  in integer  $\sigma$  intervals. For the blue and red components,  $1\sigma = 12.9$  and  $13.7 \text{ mJy/beam km/s}$ , respectively. The rectangle indicates the region from which the PV diagram in Figure 4 is calculated. The NOEMA beam is also shown in the lower left.

by (e.g., McCray & Snow 1979),

$$R = 16 \left( \frac{L_{36}}{n_0 v_{1000}} \right)^{1/4} t_6^{1/2} \text{ pc}, \quad (1)$$

where  $L_{36}$  and  $v_{1000}$  are the mechanical luminosity and wind velocity in units of  $10^{36} \text{ erg s}^{-1}$  and  $1000 \text{ km s}^{-1}$ , respectively, providing the impetus. For  $v_{1000} = 1$ , appropriate to massive star winds, this yields  $L_{36} \sim 500$ , a value fully consistent with that expected for a young,  $M_\star \sim 10^5 M_\odot$  cluster at SMC metallicity. We further confirm that the observed dynamics are inconsistent with a conventional, energy-driven bubble. In this case, the expansion velocity  $v = 0.6R/t$ , implying an age of  $0.4 \text{ Myr}$ . For an adiabatic shell growth (e.g., McCray & Snow 1979),

$$R = 27 \left( \frac{L_{36}}{n_0} \right)^{1/5} t_6^{3/5} \text{ pc}, \quad (2)$$

the same parameters imply  $L_{36} \sim 10$ , over an order of magnitude too small. Thus, *energy-driven feedback does not dominate*, supporting a catastrophic cooling scenario (Mac Low & McCray 1988; Silich et al. 2007; Krumholz & Matzner 2009). The importance of cooling is also confirmed by 3-D hydrodynamic simulations (Krause & Diehl 2014; Yadav et al. 2017). It is therefore likely that radiation dominates the SSC feedback (e.g., Freyer et al. 2003), especially if its age is  $\leq 1 \text{ Myr}$ . The extinction-corrected  $H\alpha$  luminosity is  $8.4 \times 10^{39} \text{ erg s}^{-1}$  (Micheva et al. 2017), which is about  $10\times$  larger than the total wind power inferred above. Although the bipolar morphology implies only partial shells, this does not affect the basic mechanical feedback calculations; certainly adiabatic, pressure-driven feedback is impossible with partial shells. We will quantitatively examine the possible feedback mechanisms in detail in a future work.

Alternatively, the two molecular components could be infalling, and perhaps be the remnants of two molecular clouds whose collision triggered the formation of the SSC. This scenario has been suggested for other SSCs with similar CO morphology by, e.g., Fukui et al. (2016). Figure 4 shows a position-velocity (PV) diagram for Mrk 71-A, showing the projected kinematic structure. Haworth et al. (2015) find from their simulated observations of colliding clouds that the existence of “broad bridge” material between the blue and red components is consistent with colliding clouds. The existence of emission between the blue and red components in Figure 4 is morphologically similar to their models, although our spatial resolution is relatively low. The components could also represent random accretion infall of vestigial material from the natal molecular environment.

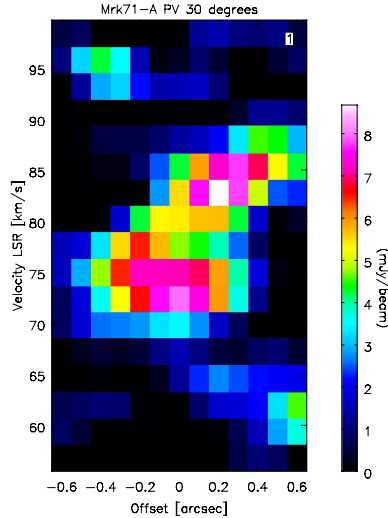


**Figure 4.** Position-velocity diagram for CO(2–1) in the region of Mrk 71-A designated in Figure 3b.

Taken as physically distinct clouds, their kinematics are also fully consistent with a virialized system, together with the SSC, as noted above. The molecular gas is likely clumpy, perhaps dominated by the two unresolved, compact, massive clouds. Since both peaks are offset from the continuum peak (Figure 3b), this enhances the likelihood that the molecular clouds do not obstruct the escape of ionizing radiation in our line of sight, consistent with the low LyC optical depth suggested by [Micheva et al. \(2017\)](#). If the clouds are infalling, then the blue component is likely to be behind the SSC, which further enhances this scenario.

Clarifying the timescale for gas retention and spatial relation to the SSC is critical for understanding the conditions for LyC escape and Green Pea-like systems. In particular, adiabatic superwinds have been suggested to be important in clearing passages for ionizing radiation (e.g., [Zastrow et al. 2013](#); [Heckman et al. 2011](#)). The action of mechanical feedback takes time, while after 3 Myr, the ionizing stellar population declines ([Dove et al. 2000](#); [Fujita et al. 2003](#)). Thus, in this model, there is significant LyC escape only in a short period dominated by classical Wolf-Rayet stars around age 3 – 5 Myr ([Zastrow et al. 2013](#)). However, Mrk 71-A is most likely younger than 3 Myr old, perhaps even by a factor of 10, and it is a strong candidate LCE, quantitatively matching Green Pea properties in all respects, including extreme excitation and low optical depth ([Micheva et al. 2017](#)). Since we show that any mechanical feedback in this system is not energy-driven, it suggests that superwinds are not a necessary condition for LyC escape.

#### 4. CONCLUSION

In summary, our NOEMA CO(2–1) observations detect a compact,  $\sim 7$  pc,  $10^5 M_{\odot}$  molecular cloud coincident with the SSC Mrk 71-A, which is of similar mass. At face value, the implied SFE is high, on the order of 0.5, as seen in similar objects. In the extremely young, high-density star-forming conditions for Mrk 71-A, energy-driven feedback will be suppressed by strong, radiative cooling (e.g., [Silich et al. 2007](#); [Krause & Diehl 2014](#); [Yadav et al. 2017](#)). The presence of a massive, compact, molecular cloud cospatial with the SSC is fully consistent with this expectation, and we quantitatively demonstrate that any mechanical feedback from the SSC must be momentum-driven. Under these circumstances, radiation feedback from the young SSC is likely the dominant feedback mode (e.g., [Freyer et al. 2003](#); [Krumholz & Matzner 2009](#)). Given that Mrk 71-A is an extreme Green Pea analog and strong LCE candidate, our results suggest that superwinds are not necessary to clear gas for LyC escape.

The CO(2–1) data appear to show two, spatially distinct, kinematic components separated by  $11 \text{ km s}^{-1}$ . If expanding, these could be due to momentum-driven, stellar wind feedback. Conversely, the components could be colliding clouds responsible for triggering the formation of the SSC, or simply random vestigial accretion. Finally, the kinematics are also consistent with a virialized system.

We also detect the nebular continuum in Mrk 71-A, allowing accurate measurement of its absolute coordinates, and four additional molecular clouds of similar masses within 50 pc of the SSC. One is unresolved and extremely compact, but no continuum is detected.

We thank Jim Dale, Mark Krumholz, Eric Pellegrini, Linda Smith, and the anonymous referee for useful discussions. This work is based on observations carried out under project number W16BM with the IRAM NOEMA Interferometer. IRAM is supported by INSU/CNRS (France), MPG (Germany) and IGN (Spain).

*Facilities:* NOEMA, HST(WFC3)

## REFERENCES

- Amorín, R., Muñoz-Tuñón, C., Aguerri, J. A. L., & Planesas, P. 2016, *A&A* 588, A23
- Bolatto, A., Wolfire, M. & Leroy, A. 2013, *ARAA* 51, 207
- Cardamone, C. et. al., 2009, *MNRAS*, 399, 1191
- Chevalier, R. A. & Clegg, A. W. 1985, *Nature*, 317, 44
- Chomiuk, L. & Wilcots, E. M. 2009, *AJ* 137, 3869
- Dale, J. E., 2015, *NewAR*, 68, 1
- Dove, J. B., Shull, J. M., & Ferrara, A. 2000, *ApJ* 531, 846
- Drissen, L., Roy, J.-R., Robert, C., & Devost, D. 2000, *ApJ* 119, 688
- Freyer, T., Hensler, G., & Yorke, H. W. 2003, *ApJ*, 594, 888
- Fujita, A., Martin, C. L., Mac Low, M.-M., & Abel, T. 2009, *ApJ* 599, 50
- Fukui, Y., Torii, K., Ohama, A., et al. 2016, *ApJ* 820, 26
- Gratton, R. G., Carretta, E., & Bragaglia, A. 2012, *A&ARv* 20, 50
- Guseva, N. G., Izotov, Y. I., & Thuan, T. X., *ApJ* 644, 890
- Haworth, T. J., Tasker, E. J., Fukui, Y., et al. 2015, *MNRAS* 450, 10
- Heckman, T. M., Borthakur, S., Overzier, R., et al. 2011, *ApJ* 730, 5
- González-Delgado, R. M., et al. 1994, *ApJ* 437, 239
- Herrera, C. N. & Boulanger, F. 2017, *A&A* 600, A139
- Izotov, Y. I. et. al., 2011, *ApJ*, 728, 161
- Izotov, Y. I. et. al., 2016a, *Nature*, 529, 178
- Izotov, Y. I. et. al., 2016b, *MNRAS*, 461, 3683
- James, B. L., Auger, M., Aloisi, A., Calzetti, D., & Kewley, L. 2016, *ApJ*, 816, 40
- Jaskot, A. E. & Oey, M. S., 2013, *ApJ*, 766, 91
- Krause, M. G. H., & Diehl, R. 2014, *ApJL* 794, L21
- Kruijssen, J. M. D. 2012, *MNRAS* 426, 3008
- Krumholz, M. R. & Matzner, C. D. 2009, *ApJ* 703, 1352
- Leroy, A., Bolatto, A., Gordon, K. et al. 2011, *ApJ* 737, 12
- MacLaren, I., Richardson, K. M., & Wolfendale, A. W. 1988, *ApJ* 333, 821
- Mac Low, M.-M., & McCray, R. 1988, *ApJ* 324, 776
- Martínez-González, S., Silich, S., & Tenorio-Tagle, G. 2014, *ApJ* 785, 164
- McCray, R. & Snow, T. P. 1979, *ARA&A* 17, 213
- Micheva, G., Oey, M. S., Jaskot, A. E., & James, B. L. 2017, *ApJ*, in press; arXiv:1704.01678
- Silich, S. & Tenorio-Tagle, G. & Muñoz-Tuñón, C., 2007, *ApJ* 669, 952
- Silich, S. & Tenorio-Tagle, G. 2017, *MNRAS* 465, 1375
- Smith, L. J., et al. 2006, *ApJ* 370, 513
- Sorai, K. et. al., 2001, *ApJ* 551, 794
- Tolstoy, E. et. al., 1995, *AJ*, 110, 1640
- Turner, J. L. et. al., 2015, *Nature*, 519, 331
- Turner, J. L., et al. 2017, arXiv:1706.09944
- Weaver, R., McCray, R., Castor, J., Shapiro, P., & Moore, R. 1977, *ApJ* 218, 377
- Yadav, N., Mukherjee, D., Sharma, P., & Nath, B. B. 2017, *MNRAS* 465, 1720
- Zastrow, J., Oey, M. S., Veilleux, S., & McDonald, M. 2013, *ApJ* 779, 76